Optimization of bodies with locally periodic microstructure by varying the periodicity pattern

Cristian Barbarosie
Anca-Maria Toader

e-mail : {barbaros,amtan}@ptmat.fc.ul.pt

Preprint CMAF Pre-010 (2013)
http://cmaf.ptmat.fc.ul.pt/preprints.html

July 17, 2013

Abstract

This paper describes a numerical study of the optimization of elastic bodies featuring a locally periodic microscopic pattern. Our approach makes the link between the microscopic level and the macroscopic one. It adds a new component (variation of the periodicity pattern) to previously published works by the same authors. Two-dimensional linearly elastic bodies are considered; the same techniques can be applied to three-dimensional bodies. Homogenization theory is used to describe the macroscopic (effective) elastic properties of the body. The macroscopic domain is divided in (rectangular) finite elements and in each of them the microstructure is supposed to be periodic; the periodic pattern is allowed to vary from element to element. Each periodic microstructure is discretized using a finite element mesh on the periodicity cell, by identifying the opposite sides of the cell in order to handle the periodicity conditions in the cellular problem. Shape, topology and periodicity optimization are used at the microscopic level, following an alternate directions algorithm. Numerical examples are presented, in which a cantilever is optimized for different load cases, one of them being multi-load. The problem is numerically heavy, since the optimization of the macroscopic problem is performed by optimizing in simultaneous hundreds or even thousands of periodic structures, each one using its own finite element mesh on the periodicity cell. Parallel computation is used in order to alleviate the computational burden.

Keywords : shape optimization, topology optimization, alternate directions algorithm, locally periodic homogenization, cellular problem, parallel computation

1 Introduction

The main motivation of the present paper comes from the study of bodies having locally periodic microstructure and optimization of their macroscopic properties, in the context of linearized elasticity. A body having locally periodic microstructure is a body whose material coefficients vary at a microscopic scale, and this variation is locally periodic in the sense that, around each point of the body, the material coefficients vary according to a periodic pattern. This pattern changes from point to point (at the macroscopic scale). Homogenization theory allows one to accurately describe the macroscopic behaviour of such a body by means of so-called cellular problems, which are elliptic PDEs subject to periodicity conditions, see e.g. [1], [2]. Porous materials, that is, bodies with locally periodic infinitesimal perforations, can be described in a similar manner, see [3].

In [4], the authors have presented an algorithm for optimization of locally periodic structures. This algorithm links the microsopic level with the macroscopic problem. At the microscopic level, the optimization process described in [4] focuses on the shape of the microscopic hole and on its topology (that is, the number of its connected components). However, the periodicity group (or, more precisely, the two vectors defining the periodicity cell) was kept fixed along the optimization process.

In the present paper, the authors present new results obtained by varying the vectors defining the periodicity. The structure thus obtained has much more freedom do adapt itself to the macroscopic loads, by adjusting the periodicity cell's aspect and orientation along the optimization process. In order to compute the desired variation of the vectors defining the periodicity, the authors have computed the derivatives of the homogenized elastic coefficients with respect to these two vectors. These derivatives are then linked with the derivative of the macroscopic objective functional with respect to the elastic coefficients.

Preliminary results were presented in [5] and [6].

The layout of the paper is as follows. Section 2 presents the mathematical background on periodic microstructures. Section 3 focuses on the computation of the derivatives of the homogenized elastic coefficents with respect to the geometric parameters defining the microstructure, with special emphasis on the derivative with respect to the vectors defining the periodicity pattern. Section 4 extends these notions and results to locally periodic microstructures. Section 5 describes the optimization process, while in Section 6 some numerical examples are presented.

2 Periodic microstructures

As a preliminary for describing mathematically the notion of body having locally periodic microsctructure, we briefly recall some notations and results on periodic microstructures. For more details, see [7].

Consider a parallelogram Y in $\mathbb{R}^2$ which defines the periodicity of the mi-

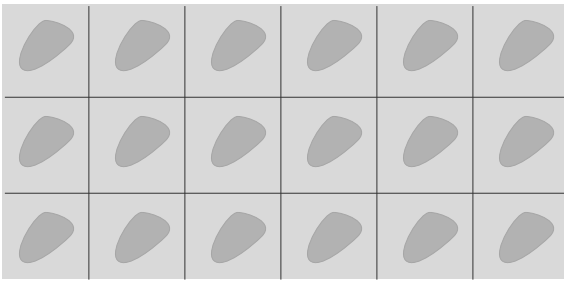

Figure 1: Periodic mixture of two materials

crostructure. Often Y is taken to be the unit square for the sake of simplicity, but in the present work Y will be a general parallelogram defined by two linearly independent vectors $\vec{g}_1, \vec{g}_2 \in \mathbb{R}^2$:

$$Y = \left\{ s_1 \vec{g}_1 + s_2 \vec{g}_2 : s_1, s_2 \in [0,1] \right\} \tag{1}$$

A periodic microstructure is a body whose material coefficients (i.e., for the case of linear elasticity, its rigidity tensor) varies according to a periodic pattern C, which is a Y-periodic fourth-order tensor field $\mathsf{C} : \mathbb{R}^2 \to \mathbb{R}^{16}$. Typically, but not necessarily, the pattern tensor field C takes only two values, modeling a periodic mixture between two given component materials (see Figure 1).

The effective (macroscopic) behaviour of the body is described by the so-called homogenized elastic tensor, denoted by C^H and defined in terms of solutions of elliptic partial differential equations subject to periodicity conditions. More precisely, for a given macroscopic strain (represented by a symmetric 2×2 matrix A), consider the problem

$$\begin{cases} -\mathrm{div}(\mathsf{C}\,\epsilon(w_{\mathsf{A}})) = 0 \text{ in } \mathbb{R}^2 \\ w_{\mathsf{A}}(y) = \mathsf{A}y + \phi_{\mathsf{A}}(y), \quad \text{with } \phi_{\mathsf{A}}\ Y-\text{periodic}, \end{cases} \tag{2}$$

known in homogenization theory as *cellular problem*. Here, ϵ represents the symmetric part of the gradient. A function ϕ is said to be Y-periodic if $\phi(y + \vec{g}_i) = \phi(y)$ for $i \in \{1, 2\}$.

The solution w_{A} of the above problem depends (linearly) on the matrix A. Consequently, the matrix σ defined by

$$\sigma = \frac{1}{|Y|} \int_Y \mathsf{C}\,\epsilon(w_{\mathsf{A}})\,,$$

representing the macroscopic stress associated to w_{A}, depends linearly on the macroscopic strain A and this dependency defines the homogenized elastic tensor C^H through $\mathsf{C}^H\mathsf{A} = \sigma$, that is,

$$\mathsf{C}^H\mathsf{A} = \frac{1}{|Y|} \int_Y \mathsf{C}\,\epsilon(w_{\mathsf{A}})\,. \tag{3}$$

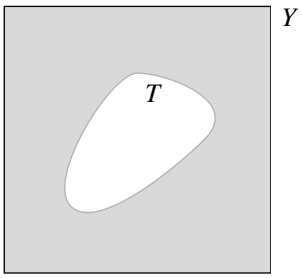

Figure 2: Periodicity cell with model hole (zoomed)

In the above, $|Y|$ denotes the area of the periodicity cell Y. An equivalent definition of C^H can be given in terms of energy type products : for two given symmetric matrices A and B, one has

$$\langle \mathsf{C}^H \mathsf{A}, \mathsf{B} \rangle = \frac{1}{|Y|} \int_Y \langle \mathsf{C}\, \epsilon(w_\mathsf{A}), \epsilon(w_\mathsf{B}) \rangle \, .$$

Note that, for a function w_A of the form $w_\mathsf{A}(y) = \mathsf{A}y + \phi_\mathsf{A}(y)$, with ϕ_A Y-periodic, one has

$$\mathsf{A} = \frac{1}{|Y|} \int_Y \epsilon(w_\mathsf{A}) \tag{4}$$

(see in [7] Lemma 1 and its consequences).

This can be expressed in a more concise form by introducing the set of *linear plus periodic* functions denoted by

$$LP = \{ w : \mathbb{R}^2 \mapsto \mathbb{R}^2 \mid w(y) = \mathsf{A}y + \phi(y) \text{ with } \mathsf{A}\ 2\times 2 \text{ matrix and } \phi\ Y\text{-periodic} \} \, . \tag{5}$$

Functions $w \in LP$ are characterized by the property

$$w(y + \vec{g}_i) = w(y) + A\vec{g}_i \, , \ i = 1, 2 \, . \tag{6}$$

The cellular problem (2) may be written in strain formulation as follows:

$$\left\{ \begin{array}{c} w_\mathsf{A} \in LP \\ -\mathrm{div}(\mathsf{C}\, \epsilon(w_\mathsf{A})) = 0 \text{ in } \mathbb{R}^2 \\ \frac{1}{|Y|} \int_Y \epsilon(w_\mathsf{A}) = \mathsf{A} \, , \end{array} \right. \tag{7}$$

where A is a prescribed strain matrix.

The case of porous structures, that is, infinitesimal perforations in a given material, can be treated in a similar way (see [7, Section 4]). Consider a model hole, which is a compact set $T \subset Y$ (see Figure 2), where Y is the periodicity cell. The cellular problem describing the behaviour of this perforated material is defined on the perforated space, denoted by $\mathbb{R}^2_{\mathrm{perf}}$, and a Neumann boundary condition is imposed on the boundary of the model hole.

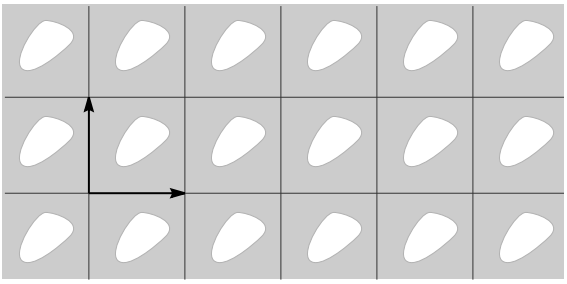

Figure 3: Periodically perforated plane $\mathbb{R}^2_{\text{perf}}$

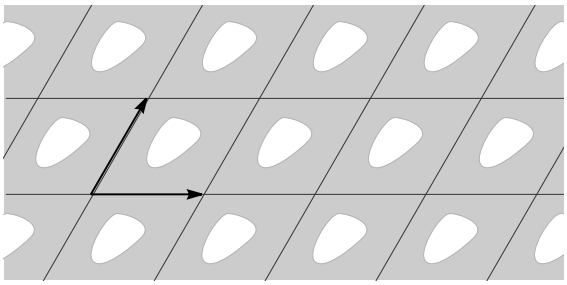

Figure 4: Periodically perforated plane $\mathbb{R}^2_{\text{perf}}$ for another cell

The perforated space is obtained from $\mathbb{R}^2$ by removing translations of the model hole (see Figures 3 and 4) :

$$\mathbb{R}^2_{\text{perf}} = \mathbb{R}^2 \setminus \bigcup_{\vec{k}\in\mathbb{Z}^n} (T + k_1\vec{g}_1 + k_2\vec{g}_2)$$

The direct generalization of the cellular problem (2) for porous materials is stated below (the base material C is now considered to be constant) :

$$\begin{cases} -\text{div}(\mathsf{C}\,\epsilon(w_{\mathsf{A}})) = 0 \text{ in } \mathbb{R}^2_{\text{perf}} \\ \mathsf{C}\,\epsilon(w_{\mathsf{A}})\,\text{n} = 0 \text{ on } \partial T \\ w_{\mathsf{A}}(y) = \mathsf{A}y + \phi_{\mathsf{A}}(y), \quad \phi_{\mathsf{A}} \text{ periodic function.} \end{cases} \tag{8}$$

The homogenized tensor C^H can be defined as

$$\mathsf{C}^H\mathsf{A} = \frac{1}{|Y|}\int_{Y\setminus T} \mathsf{C}\,\epsilon(w_{\mathsf{A}})$$

or

$$\langle \mathsf{C}^H\mathsf{A}, \mathsf{B}\rangle = \frac{1}{|Y|}\int_{Y\setminus T} \langle \mathsf{C}\,\epsilon(w_{\mathsf{A}}), \epsilon(w_{\mathsf{B}})\rangle\,.$$

Remark 1 *Note that, through careful interpretetation, problem (8) makes sense even if the model hole T exits partially the periodicity cell Y, as long as it does*

not touch any of its translations $T + \vec{k}$, $\vec{k} \in \mathbb{Z}^n$, $\vec{k} \neq \vec{0}$. *This is important since, in the optimization process, the model hole often crosses the boundary of* Y.

Remark 2 *In Figures 2, 3 and 4, the model hole* T *was chosen to be connected. But there is no difficulty in considering a model hole with several connected components.*

3 Derivatives of the homogenized coefficients

The homogenized elastic tensor C^H depends, of course, on the geometric parameters defining the periodic structure under consideration : the shape and topology of the model hole T, as well as the periodicity pattern. In order to use gradient-based optimization algorithms, the derivatives of these dependencies must be computed.

The aim of this section is the computation of the derivative of the homogenized tensor with respect to the periodicity pattern (at the end of the section we recall the fomulae for the shape and topology derivatives). This periodicity pattern is given by the aspect and orientation of the periodicity cell Y, or, equivalently, by the two vectors $\vec{g}_1$ and $\vec{g}_2$ defining Y, see formula (1). Our goal is to compute the derivative of the homogenized elastic coefficients (components of the tensor C^H) with respect to the vectors $\vec{g}_1$ and $\vec{g}_2$.

We shall analyse the case of a mixture of materials, governed by the system (2) or, equivalently, (7). The case of porous materials, governed by the system (8), can be treated in a similar manner.

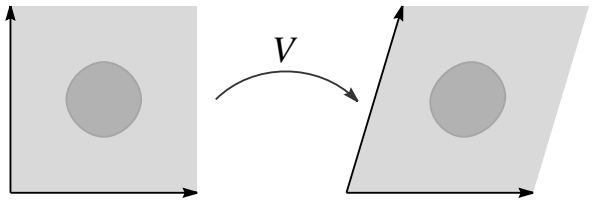

Figure 5: Change in the periodicity pattern

Consider a linear application V (see Figure 5) that transforms the periodicity cell Y in $\tilde{Y}$ generated by the vectors $\vec{\tilde{g}}_1 = V(\vec{g}_1)$ and $\vec{\tilde{g}}_2 = V(\vec{g}_2)$. The corresponding fourth-order tensor field $\tilde{C}$ verifies $\tilde{\mathsf{C}}(V(y)) = \mathsf{C}(y)$. The homogenized coefficients $\tilde{\mathsf{C}}^H$ for the deformed configuration are defined by evaluating, for two given symmetric matrices A and B, the energy-type quantity

$$\langle \tilde{\mathsf{C}}^H \mathsf{A}, \mathsf{B} \rangle = \frac{1}{|\tilde{Y}|} \int_{\tilde{Y}} \langle \tilde{\mathsf{C}}(z)\, \epsilon(\tilde{w}_{\mathsf{A}})(z), \epsilon(\tilde{w}_{\mathsf{B}})(z) \rangle \, dz.$$

where $\tilde{w}_{\mathsf{A}}$ and $\tilde{w}_{\mathsf{B}}$ are the solutions of problem (7) in the deformed configuration.

By changing the integration domain to Y, the above expression writes as

$$\langle \tilde{\mathsf{C}}^H \mathsf{A}, \mathsf{B} \rangle = \frac{1}{|\tilde{Y}|} \int_Y \langle \tilde{\mathsf{C}}(V(y))\, \epsilon(\tilde{w}_{\mathsf{A}})(V(y)), \epsilon(\tilde{w}_{\mathsf{B}})(V(y)) \rangle |det(V)| dy,$$

and having in mind that $\tilde{\mathsf{C}}(V(y)) = \mathsf{C}(y)$ and $|\tilde{Y}| = |det \nabla V||Y| = |detV||Y|$,

$$\langle \tilde{\mathsf{C}}^H \mathsf{A}, \mathsf{B} \rangle = \frac{1}{|Y|} \int_Y \langle \mathsf{C}(y)\, \epsilon(\tilde{w}_{\mathsf{A}})(V(y)), \epsilon(\tilde{w}_{\mathsf{B}})(V(y)) \rangle dy.$$

By taking advantage of the symmetry properties of the elastic tensor C, the quantity $\langle \tilde{\mathsf{C}}^H \mathsf{A}, \mathsf{B} \rangle$ can be written in the form

$$\langle \tilde{\mathsf{C}}^H \mathsf{A}, \mathsf{B} \rangle = \frac{1}{|Y|} \int_Y \mathsf{C}_{ijkl}(y) \frac{\partial \tilde{w}^i_{\mathsf{A}}}{\partial z_j}(V(y)) \frac{\partial \tilde{w}^k_{\mathsf{B}}}{\partial z_l}(V(y))\, dy.$$

In order to express the above quantity in terms of functions defined on the original configuration Y, we introduce the functions $\bar{w}_{\mathsf{A}}(y) = \tilde{w}_{\mathsf{A}}(V(y))$ and $\bar{w}_{\mathsf{B}}(y) = \tilde{w}_{\mathsf{B}}(V(y))$. One has then $\tilde{w}_{\mathsf{A}}(z) = \bar{w}_{\mathsf{A}}(W(z))$, with $W = V^{-1}$, and thus $\dfrac{\partial \tilde{w}^i_{\mathsf{A}}}{\partial z_j}(z) = \dfrac{\partial \bar{w}^i_{\mathsf{A}}}{\partial y_m}(W(z))\, \dfrac{\partial W^m}{\partial z_j}(z)$ and similarly $\dfrac{\partial \tilde{w}^k_{\mathsf{B}}}{\partial z_l}(z) = \dfrac{\partial \bar{w}^k_{\mathsf{B}}}{\partial y_p}(W(z))\, \dfrac{\partial W^p}{\partial z_l}(z)$. Due to the linear character of V and W, $\dfrac{\partial W^m}{\partial z_j}(z) = W_{mj}$ and $\dfrac{\partial W^p}{\partial z_l}(z) = W_{pl}$, hence

$$\langle \tilde{\mathsf{C}}^H \mathsf{A}, \mathsf{B} \rangle = \frac{1}{|Y|} \int_Y \mathsf{C}_{ijkl} \frac{\partial \bar{w}^i_{\mathsf{A}}}{\partial y_m} W_{mj} \frac{\partial \bar{w}^k_{\mathsf{B}}}{\partial y_p} W_{pl}\, dy.$$

It is now possible to study the (infinitesimal) variations induced in the quantity $\langle \tilde{\mathsf{C}}^H \mathsf{A}, \mathsf{B} \rangle$ by infinitesimal variations of V. The prefix δ will be used to denote an infinitesimal variation of the quantity following it. Recall that the matrices A and B are fixed, as well as the elastic tensor C of the (undeformed) mixture. Thus :

$$\begin{aligned}\langle \delta\tilde{\mathsf{C}}^H \mathsf{A}, \mathsf{B} \rangle = {} & \frac{1}{|Y|} \int_Y \mathsf{C}_{ijkl}\, \delta \frac{\partial \bar{w}^i_{\mathsf{A}}}{\partial y_m} W_{mj} \frac{\partial \bar{w}^k_{\mathsf{B}}}{\partial y_p} W_{pl}\, dy + \frac{1}{|Y|} \int_Y \mathsf{C}_{ijkl} \frac{\partial \bar{w}^i_{\mathsf{A}}}{\partial y_m}\, \delta W_{mj} \frac{\partial \bar{w}^k_{\mathsf{B}}}{\partial y_p} W_{pl}\, dy + \\ & + \frac{1}{|Y|} \int_Y \mathsf{C}_{ijkl} \frac{\partial \bar{w}^i_{\mathsf{A}}}{\partial y_m} W_{mj}\, \delta \frac{\partial \bar{w}^k_{\mathsf{B}}}{\partial y_p} W_{pl}\, dy + \frac{1}{|Y|} \int_Y \mathsf{C}_{ijkl} \frac{\partial \bar{w}^i_{\mathsf{A}}}{\partial y_m} W_{mj} \frac{\partial \bar{w}^k_{\mathsf{B}}}{\partial y_p}\, \delta W_{pl}\, dy\,.\end{aligned}$$

The symbol δ commutes with the partial derivatives, hence

$$\begin{aligned}\langle \delta\tilde{\mathsf{C}}^H \mathsf{A}, \mathsf{B} \rangle = {} & \frac{1}{|Y|} \int_Y \mathsf{C}_{ijkl} \frac{\partial(\delta \bar{w}^i_{\mathsf{A}})}{\partial y_m} W_{mj} \frac{\partial \bar{w}^k_{\mathsf{B}}}{\partial y_p} W_{pl}\, dy + \frac{1}{|Y|} \int_Y \mathsf{C}_{ijkl} \frac{\partial \bar{w}^i_{\mathsf{A}}}{\partial y_m}\, \delta W_{mj} \frac{\partial \bar{w}^k_{\mathsf{B}}}{\partial y_p} W_{pl}\, dy + \\ & + \frac{1}{|Y|} \int_Y \mathsf{C}_{ijkl} \frac{\partial \bar{w}^i_{\mathsf{A}}}{\partial y_m} W_{mj} \frac{\partial(\delta \bar{w}^k_{\mathsf{B}})}{\partial y_p} W_{pl}\, dy + \frac{1}{|Y|} \int_Y \mathsf{C}_{ijkl} \frac{\partial \bar{w}^i_{\mathsf{A}}}{\partial y_m} W_{mj} \frac{\partial \bar{w}^k_{\mathsf{B}}}{\partial y_p}\, \delta W_{pl}\, dy\,.\end{aligned}$$

Expressing the variation of $W = V^{-1}$ in terms of the variation of V is a mere exercise of calculus :

$$V_{ij} W_{jk} = \delta_{ik} \quad \Longrightarrow \quad \delta V_{ij} W_{jk} + V_{ij}\, \delta W_{jk} = 0 \quad \Longrightarrow \quad \delta W_{ij} = -W_{ik}\, \delta V_{kl}\, W_{lj}$$

We now localize the computations, that is, we compute the desired derivative around the point $V = \mathrm{Id}$ (the identity matrix). By doing this, W becomes also Id, and $\tilde{w}_{\mathsf{A}} = \bar{w}_{\mathsf{A}} = w_{\mathsf{A}}$. We shall also switch the notation from $\delta\tilde{\mathsf{C}}^H$ to $D_P\mathsf{C}^H$ (the derivative of C^H with respect to periodicity). Thus :

$$\langle D_P\mathsf{C}^H\mathsf{A},\mathsf{B}\rangle = \frac{1}{|Y|}\int_Y \mathsf{C}_{ijkl}\frac{\partial(\delta\bar{w}^i_{\mathsf{A}})}{\partial y_j}\frac{\partial w^k_{\mathsf{B}}}{\partial y_l}\,dy - \frac{1}{|Y|}\int_Y \mathsf{C}_{ijkl}\frac{\partial w^i_{\mathsf{A}}}{\partial y_m}\,\delta V_{mj}\frac{\partial w^k_{\mathsf{B}}}{\partial y_l}\,dy + \\ + \frac{1}{|Y|}\int_Y \mathsf{C}_{ijkl}\frac{\partial w^i_{\mathsf{A}}}{\partial y_j}\frac{\partial(\delta\bar{w}^k_{\mathsf{B}})}{\partial y_l}\,dy - \frac{1}{|Y|}\int_Y \mathsf{C}_{ijkl}\frac{\partial w^i_{\mathsf{A}}}{\partial y_j}\frac{\partial w^k_{\mathsf{B}}}{\partial y_p}\,\delta V_{pl}\,dy\,.$$

Due to a compensated compactness result (e.g. Lemma 1.3.1 in [1] adapted to the particular case of periodic fields), the first and third parcels in the expression above can be written as products of averages :

$$\langle D_P\mathsf{C}^H\mathsf{A},\mathsf{B}\rangle = \frac{1}{|Y|}\int_Y \frac{\partial(\delta\bar{w}^i_{\mathsf{A}})}{\partial y_j}\,dy\;\frac{1}{|Y|}\int_Y \mathsf{C}_{ijkl}\,\frac{\partial w^k_{\mathsf{B}}}{\partial y_l}\,dy - \frac{1}{|Y|}\int_Y \mathsf{C}_{ijkl}\frac{\partial w^i_{\mathsf{A}}}{\partial y_m}\,\frac{\partial w^k_{\mathsf{B}}}{\partial y_l}\,dy\;\delta V_{mj} + \\ + \frac{1}{|Y|}\int_Y \mathsf{C}_{ijkl}\,\frac{\partial w^i_{\mathsf{A}}}{\partial y_j}\,dy\;\frac{1}{|Y|}\int_Y \frac{\partial(\delta\bar{w}^k_{\mathsf{B}})}{\partial y_l}\,dy - \frac{1}{|Y|}\int_Y \mathsf{C}_{ijkl}\,\frac{\partial w^i_{\mathsf{A}}}{\partial y_j}\,\frac{\partial w^k_{\mathsf{B}}}{\partial y_p}\,dy\;\delta V_{pl}\,.$$

We stress that the second and fourth parcels cannot be written in the same way.

We now apply two properties already refered in Section 2, equations (3) and (4). Note that, since $\bar{w}_{\mathsf{A}}$ is a linear plus periodic function whose linear part is AV, $\delta\bar{w}_{\mathsf{A}}$ is a linear plus periodic function whose linear part is $A\delta V$. Similarly, the linear part of $\delta\bar{w}_{\mathsf{B}}$ is $B\,\delta V$, hence

$$\langle D_P\mathsf{C}^H\mathsf{A},\mathsf{B}\rangle = \mathsf{A}_{i\alpha}\,\delta V_{\alpha j}\,\mathsf{C}^H_{ijkl}\,\mathsf{B}_{kl} - \frac{1}{|Y|}\int_Y \mathsf{C}_{ijkl}\,\frac{\partial w^i_{\mathsf{A}}}{\partial y_m}\,\frac{\partial w^k_{\mathsf{B}}}{\partial y_l}\,dy\;\delta V_{mj} + \\ + \mathsf{C}^H_{ijkl}\,\mathsf{A}_{ij}\,B_{k\alpha}\,\delta V_{\alpha l} - \frac{1}{|Y|}\int_Y \mathsf{C}_{ijkl}\,\frac{\partial w^i_{\mathsf{A}}}{\partial y_j}\,\frac{\partial w^k_{\mathsf{B}}}{\partial y_p}\,dy\;\delta V_{pl}\,. \qquad (9)$$

The above formula is ready for implementation, since it gives the derivative of the homogenized tensor in terms of computable quantities multiplying (components of) δV. By choosing the matrices A and B in a basis of symmetric matrices, one may write equation (9) in a compact form :

$$D_P\mathsf{C}^H = \mathbb{P}\,\delta V\,, \qquad (10)$$

where $\mathbb{P}$ is a sixth order tensor describing the sensitivity of C^H with respect to the periodicity pattern.

We state here the formulae of the shape and topology derivatives; the interested reader may find more details in [7, Sections 5 and 6].

Consider first shape variations, given by an infinitesimal deformation τ of the model hole T, see Figure 6. Then, the corresponding variations in the homogenized tensor are described by

$$\langle D_S\mathsf{C}^H\mathsf{A},\mathsf{B}\rangle = \frac{1}{|Y|}\int_{\partial T}\left[2\mu\langle\epsilon_y(w_{\mathsf{A}}),\epsilon_y(w_{\mathsf{B}})\rangle + \lambda\mathrm{tr}(\epsilon_y(w_{\mathsf{A}}))\mathrm{tr}(\epsilon_y(w_{\mathsf{B}}))\right]\langle\vec{\tau},\mathrm{n}\rangle\,ds(y)\,, \qquad (11)$$

where ds denotes the superficial measure on ∂T, while λ and μ are the Lamé coefficients of the (constant) base material tensor C. See equation (32) in [7].

By choosing the matrices A and B in a basis of symmetric matrices, one may write equation (11) in a compact form:

$$D_S \mathsf{C}^H = \int_{\partial T} \mathbb{S}(y)\, \langle \vec{r}, \mathrm{n} \rangle \, ds(y)\,, \tag{12}$$

where $\mathbb{S}$ is a fourth order tensor describing the shape sensitivity of C^H.

The sensitivity of C^H with respect to topology variations, that is, with respect to the nucleation of an infinitesimal hole at an arbitrary location y in the periodicity cell, is described by

$$\langle D_T \mathsf{C}^H(y)\mathsf{A}, \mathsf{B} \rangle = -\frac{\pi}{|Y|} \frac{\lambda + 2\mu}{\lambda + \mu} \Big[4\mu \langle \epsilon_y(w_\mathsf{A}), \epsilon_y(w_\mathsf{B}) \rangle + \frac{\lambda^2 + 2\lambda\mu - \mu^2}{\mu} \operatorname{tr}(\epsilon_y(w_\mathsf{A})) \operatorname{tr}(\epsilon_y(w_\mathsf{B})) \Big](y)\,,$$

see equation (24) in [7]. This can be again expressed in a compact form

$$D_T C^H(y) = -\mathbb{T}(y) \tag{13}$$

where $\mathbb{T}$ is a fourth order tensor describing the topology sensitivity of C^H.

4 Locally periodic microstructures

We call "locally periodic" a microsctructure which, in the neighbourhood of each point of the macroscopic domain, has a periodic character. This periodic microgeometry can vary from point to point (at the macroscopic level), as described in [4, Section 3].

For mixtures of materials, this amounts to letting the pattern tensor field C depend on both x (the macroscopic variable) and y (the microscopic variable). Note that in [4] the periodicity cell was kept fixed and thus it did not depend on x. In the present work the periodicity pattern is allowed to vary from (macroscopic) point to point, and is also varied along the optimization process. Thus, the periodicity cell depends on the macroscopic variable x, and is denoted by $Y(x)$.

The cellular problem (2) depends on x as a parameter :

$$\begin{cases} -\mathrm{div}_y\big(\mathsf{C}(x,y)\, \epsilon_y(w_\mathsf{A}(x,y))\big) = 0 \text{ in } \mathbb{R}^n \\ w_\mathsf{A}(x,y) = \mathsf{A}y + \phi_\mathsf{A}(x,y), \quad \text{with } \phi_\mathsf{A}(x,\cdot)\ Y(x)\text{−periodic}, \end{cases} \tag{14}$$

The homogenized elastic tensor C^H depends now on x and is defined by

$$\langle \mathsf{C}^H(x)\mathsf{A}, \mathsf{B} \rangle = \frac{1}{|Y(x)|} \int_{Y(x)} \langle \mathsf{C}(x,y) \epsilon_y(w_\mathsf{A}(x,y)), \epsilon_y(w_\mathsf{B}(x,y)) \rangle \, dy\,,$$

where A and B are two arbitrary strain matrices.

A locally periodic porous material is described in a similar manner. The model hole T now varies with x and shall be denoted by $T(x)$.

The corresponding perforated space will be denoted by $\mathbb{R}^n_{\rm perf}(x)$

$$\mathbb{R}^n_{\rm perf}(x) = \mathbb{R}^n \setminus \bigcup_{\vec{k}\in\mathbb{Z}^n} (T(x) + k_1\vec{g}_1(x) + k_2\vec{g}_2(x))$$

The base material C is now considered to be constant. The cellular problem (8) becomes

$$\begin{cases} -\mathrm{div}_y\big(\mathsf{C}\,\epsilon_y(w_{\mathsf{A}}(x,y))\big) = 0 \text{ in } \mathbb{R}^n_{\rm perf}(x) \\ \mathsf{C}\,\epsilon_y(w_{\mathsf{A}}(x,y))\,\mathrm{n} = 0 \text{ on } \partial T(x) \\ w_{\mathsf{A}}(x,y) = \mathsf{A}y + \phi_{\mathsf{A}}(x,y), \quad \text{with } \phi_{\mathsf{A}}\ Y(x)-\text{periodic.} \end{cases} \tag{15}$$

The homogenized ellastic tensor $\mathsf{C}^H(x)$ is defined by

$$\langle \mathsf{C}^H(x)\mathsf{A},\mathsf{B}\rangle = \frac{1}{|Y(x)|}\int_{Y(x)\setminus T(x)} \langle \mathsf{C}\,\epsilon_y(w_{\mathsf{A}}(x,y)), \epsilon_y(w_{\mathsf{B}}(x,y))\rangle\, dy\,, \tag{16}$$

where A and B are two arbitrary strain matrices.

The behaviour of the macroscopic body is described by the homogenized elastic tensor $\mathsf{C}^H(x)$. More precisely, suppose that the macroscopic body occupies the domain $\Omega \subset \mathbb{R}^n$, that the boundary of Ω is split in two parts (the Neumann part Γ_N and the Dirichlet part Γ_D) and that the body is subject to the superficial force g. Then, the state of deformation of the body is described by the solution u of

$$\begin{cases} -\mathrm{div}_x(\mathsf{C}^H\epsilon_x(u)) = 0 & \text{in} \quad \Omega \\ u = 0 & \text{on} \quad \Gamma_D \\ (\mathsf{C}^H\epsilon_x(u))\,\mathrm{n} = g & \text{on} \quad \Gamma_N\,. \end{cases} \tag{17}$$

Remark 3 *One may wonder how microstructures with different periodicity patterns can be glued together in order to manufacture a macroscopic body with the desired properties. This is a pertinent question,*[1] *but it is outside the scope of the present paper. In the present work, we simply assume that the microstructures are truly infinitesimal and one can glue together pieces of homogenized materials with no difficulty.*

Remark 4 *Actually, the objection risen in Remark 3 applies, although to a lesser extent, even to the context of locally periodic microstructures with constant periodicity pattern, like the ones studied in [4]. Indeed, perforations of different shapes can sometimes be difficult to glue together.*

The expressions of the derivatives of the homogenized elastic coefficients, obtained in Section 3 for periodic microstructures, are directly generalized for locally periodic microstructures. The only difference is that now a parameter x appears in the formulae; thus, equations (10), (12) and (13) become :

$$D_P\mathsf{C}^H(x) = \mathbb{P}(x)\,\delta V\,, \tag{18}$$

$$D_S\mathsf{C}^H(x) = \int_{\partial T} \mathbb{S}(x,y)\,\langle\vec{\tau},\mathrm{n}\rangle\, ds(y)\,, \tag{19}$$

$$D_T C^H(x,y) = -\mathbb{T}(x,y) \tag{20}$$

[1] See e.g. [9] for an approach to this question.

5 Optimization process

The aim of the present paper is to optimize macroscopic properties of the body under study, by varying the details of its locally periodic microstructure, more specifically, by varying the shape and topology of the holes $T(x)$, as well as their periodicity pattern.

Consider an objective functional Φ depending on the solution u of problem (17). A typical example is the minimization of the compliance of the body

$$\Phi = \frac{1}{2}\int_{\Gamma_N} gu = \frac{1}{2}\int_\Omega \langle \mathsf{C}^H \epsilon_x(u), \epsilon_x(u)\rangle = \int_{\Gamma_N} gu - \frac{1}{2}\int_\Omega \langle \mathsf{C}^H \epsilon_x(u), \epsilon_x(u)\rangle \quad (21)$$

Usually, there is also a constraint on the volume of material:

$$V = \int_\Omega \theta\,, \quad (22)$$

where

$$\theta(x) = \frac{|Y(x)\setminus T(x)|}{|Y(x)|} = 1 - \frac{|T(x)|}{|Y(x)|}$$

is the local material density.

Remark 5 *Note that there is a slight difference (a factor of two) between formula (21) and the definition of compliance used in [4]. The reason is that the authors have learned meanwhile that definition (21) is more consistent with the mechanical notion of elastic stored energy. See also [10].*

The optimization process passes through a chain of dependencies :

$$T \mapsto \mathsf{C}^H \mapsto u \mapsto \Phi\,, \quad (23)$$

that is, to a family of cellular holes $T(x)$ one associates the homogenized tensor $\mathsf{C}^H(x)$ as defined by (16), then the macroscopic elastic deformation u as defined by (17) and finally the value of the objective functional Φ. A simpler chain of dependencies holds for the volume V of material.

Describing the variation $\delta\Phi$ of the objective functional in terms of $\delta\mathsf{C}^H$ and δu is relatively simple. It is rather difficult to eliminate δu, thus expressing $\delta\Phi$ in terms of $\delta\mathsf{C}^H$ only. For the particular case of the compliance functional defined in (21), one obtains

$$\delta\Phi = -\frac{1}{2}\int_\Omega \langle \delta\mathsf{C}^H \epsilon_x(u), \epsilon_x(u)\rangle$$

See [4, Section 4] for details, taking into account Remark 5 above.

As for the first part of the chain (23), equations (19), (20) and (18) describe the variation $\delta\mathsf{C}^H$ associated to an infinitesimal variation in each of the structural parameters : shape of the holes/inclusions, their topology, and their periodic arrangement, respectively.

An optimization algorithm is used which alternates shape, topology and periodicity optimization at the cellular level. The macroscopic domain Ω is divided into finite elements (rectangular ones in our approach, but this is not essential). In each macroscopic finite element, the microgeometry is supposed to be constant. Consequently, the homogenized elastic tensor C^H and the material density θ are also constant in each macroscopic finite element.

The cellular geometry describing the periodic microstructure in each macroscopic finite element is discretized using a (triangular) finite element mesh on the respective periodicity cell. Some of these triangles are filled with an isotropic elastic material of Lamé constants λ and μ while others are void, thus defining the model hole. This mesh is used for solving numerically the cellular problem (15). The periodicity conditions in (15) are implemented by identifying the opposite sides of Y and by keeping track of the linear part A of w_{A}. For more details, see [4], [8] and [11].

The computer implementation has three components : a FORTRAN program which deals with each of the cellular meshes and optimizes the microgeometry, a C++ program (using the `libMesh` library) which deals with the mascroscopic analysis, and a Python script which links these two programs and provides data exchange. The computation is strongly parallelized : the Python script connects to several machines and spreads cellular optimization processes, by using a regular internet link and the protocol `ssh`. For more details, see [4, Section 5].

6 Numerical examples

In order to illustrate the method, results for three examples are shown. A cantilever is considered, ocuppying a rectangle of size 1.5×1, clamped on its left side and subject to loads on its right side. This rectangle is divided in $600 = 30 \times 20$ Lagrange finite elements of type $Q9$. [2]

The base elastic material C is taken to have Young modulus $E = 1$ and Poisson coefficient $\nu = 0.3$. More specifically,

$$\mathsf{C}\epsilon = 2\mu\epsilon + \lambda(\mathrm{tr}\epsilon)I_{2\times 2}$$

with $\mu = 0.38461538$ and $\lambda = 0.576923$.

We minimize $\Phi + \Lambda V$ with Φ defined in (21) and V defined in (22). The Lagrange multiplier is always taken as $\Lambda = 66.66666$.

Remark 6 *This value of Λ is half of the Lagrange multiplier used in [4, Section 6]. This choice facilitates the comparison of the numerical results, see Remark 5 above.*

[2] In [4, Section 6], it was asserted that the macroscopic domain has dimensions 2×1. This statement was incorrect; the numerical results in both [4] and the present work are computed on a rectangular domain with size 1.5×1, divided into 600 finite elements.

The 600 cellular meshes (one per macroscopic element), are composed of triangular Lagrange $P1$ finite elements. The number of elements varies during the optimization process between 1000 and 2000 triangles per cellular mesh.

The algorithm starts with an initial guess consisting of a periodic microstructure, that is, having constant (square) periodicity cell Y and constant (circular) hole T, as shown in Figure 7. The conventions used in this Figure are: in the center, the density of material, $\theta = 0.9079239$, is drawn as a function defined in the macroscopic domain; on both sides, magnifications of the microstructure in 4 chosen points of the body are shown.

Starting with this initial structure, the microgeometry is varied. Shape, topology and periodicity optimization steps are alternated during the optimization process. No penalization of intermediate densities is applied.

Each numerical example is illustrated by two Figures. Firstly, Figures 8, 10 and 12 show the configuration of the body, the applied loads, and three graphics representing the evolution of the Lagrangean $\Phi + \Lambda V$, of the compliance Φ and of the volume of material V, as functions of the number of iterations. Note that, for comparison purposes, we have included in the Figures a dotted line describing the evolution of the Lagrangean in the previous approach, with no variation of the periodicity pattern, as in [4] (Remarks 5 and 6 above apply). Secondly, in Figures 9, 11 and 13 the optimized structure is presented, following the same conventions as in Figure 7 : in the center, the density of material, θ, is drawn as a function defined in the macroscopic domain, using levels of grey. Around this central zone, magnifications of the microstructure in 8 chosen macroscopic finite elements are shown. In the background of each zoom, the periodicity cell is drawn in grey.

Note that the homogenized tensor C^H of the optimized structure is difficult to represent, since it involves 6 scalar functions. A dynamic version of Figures 9, 11 and 13 is available at [12].

In the first example, a load of intensity 1 is applied in the middle point of the right side of the cantilever. Figure 8 shows the setting of the problem and the evolution of the Lagrangean $\Phi + \Lambda V$, of the compliance Φ and of the volume of material V, as functions of the number of iterations.

In the graphic of the Lagrangean, the continuous line shows the evolution of the Lagrangean when varying the periodicity pattern, while the dotted line shows the evolution in the previous approach, with constant periodicity cell, as described in [4] (Remarks 5 and 6 above apply). One can see that the present approach is more efficient, since it reaches a significantly lower value of the Lagrangean. Note that there are intervals where the Lagrangean is almost constant, and the volume of material is truly constant. These are the optimization steps when the periodicity pattern is varied. It is interesting that these optimization steps, which at first view do not contribute for decreasing the value of the Lagrangean, actually adjust the structure's periodicity pattern and help the subsequent optimization steps (mainly shape optimization) to decrease the value of the Lagrangean more efficiently.

Figure 9 shows the density of material, in grayscale, and eight zooms of the optimized microstructure in chosen points of the body. Note how very different

material densities are obtained : from a full material (Figure 11, zoom a) to an almost empty cell (Figure 11, zoom f). Note also how very different microgeometries are obtained. In Figure 9, zooms c and e we see structures close to rank-1 laminates, like those already obtained in [4]; however, now the laminates have much more freedom to orient themselves according to the stress in the macroscopic body. For instance, the microscructures represented in Figure 9, zooms d and e, exhibit a privileged direction having a slight slope, wich would be impossible to obtain if the periodicity cell were kept constant (square).

There is no symmetry imposed in either of the examples. The results depicted in Figure 9 present a rather good symmetry, as expected, including at the microscopic level, as shown in Figure 9, zooms g and h.

In the second example, a load of intensity 1 is applied in the lower right corner of the rectangle, see Figure 10. The optimized structure is represented in Figure 11. Some of the microstructures resemble rank-1 laminates (Figure 11, zooms b and c), others seem to mimic rank-2 laminates (Figure 11, zooms e, f and g), while others are more difficult to classify (Figure 11, zooms a, d and h).

The approach presented here is not limited to the minimization of the compliance: other, more complicated, functionals can be dealt with. The third example involves a multi-load situation. Three loads are considered, as shown in Figure 12, acting independently of each other. The objective functional is the average of the three compliances (for the three load cases) :

$$\Phi = \frac{\Phi_1 + \Phi_2 + \Phi_3}{3}$$

Results are presented in Figure 13. The optimized microstructures are somewhat more elaborated than in the previous two examples. Fewer laminates are obtained. These microstructures are required to resist well to three different states of (macroscopic) stress.

In all examples, one notices more intermediate grayscales when comparing with the respective results in [4]. Most importantly, a significantly lower value of the Lagrangean is obtained.

In some cases, the extreme flexibility of the periodicity cell becomes apparent, like in Figure 13, zoom h.

Remark 7 *The topology optimization steps do not contribute significantly to the optimization process. The authors have observed that, quite often, during a topology optimization step, a small hole is created and is later destroyed during subsequent shape optimization steps. Also, in the final, optimized, structures, it is very rare to see more than one hole in the periodicity cell. The only exception is shown in Figure 13, zoom b, where a very small hole can be seen. If the optimization process were continued, it is likely that this hole would have been destroyed by subsequent shape optimization steps.* [3]

[3] The reader should not be mislead by the complicated aspect of some of the microstructures. Even in the extreme case of Figure 13, zoom h, there is only one hole which crosses several times the boundary of the periodicity cell.

7 Conclusions and future work

The present paper presents an algorithm for the optimization of bodies having locally periodic perforations. Shape, topology and periodicity optimization steps are performed following an alternate directions approach. The scripting language `Python` was used in order to launch in parallel cellular optimization processes.

Our approach is related to free material optimization in the sense that it uses the derivative of the objective functional with respect to the homogenized elastic coefficients. The method is general : any objective functional can be treated, as long as its derivative with respect to the macroscopic material coefficients can be computed.

The numerical results are encouraging, showing good agreement with results from the literature.

The upgrade of the algorithm to three-dimensional problems is the object of on-going work. The main difficulty is the implementation of the finite element mesh on the cube with its opposite faces identified (which is equivalent to meshing the three-dimensional torus), especially its deformation and regeneration. Robust algorithms for mesh deformation and mesh regeneration in $\mathbb{R}^3$ are difficult to find.

Other directions for improving the algorithm in the future are: the implementation of a quasi-Newton algorithm in order to accelerate the convergence and the implementation of different optimization criteria. For instance, it could be interesting to impose an upper bound on the (microscopic) pointwise stress.

8 Acknowledgements

This work was supported by Fundação para a Ciência e a Tecnologia, PEst-OE/MAT/UI0209/2011.

Paulo Vieira helped with the implementation of the macroscopic analysis code in `C++`, using the finite element library `libMesh`.

For graphic creation, the authors have used the open-source softwares `xd3d` and `xgraphic`, by François Jouve, and `xfig`.

References

[1] G. Allaire, *Shape Optimization by the Homogenization Method*, Springer, Applied Mathematical Sciences 146, 2002

[2] F. Murat, L. Tartar, H-convergence, in: *Topics in the Mathematical Modelling of Composite Materials*, edited by A. Cherkaev and R. Kohn, Progress in Nonlinear Differential Equations and Their Applications, vol. 31, p. 21-43, Birkhäuser, 1997

[3] D. Cioranescu, J.S.J. Paulin, Homogenization in open sets with holes, *Journal of Mathematical Analysis and Applications*, 71(2), p. 590-607, 1979

[4] C. Barbarosie, A.-M. Toader, Optimization of bodies with locally periodic microstructre, *Mechanics of advanced materials and structures*, 19(4), p. 290-301, 2012

[5] C. Barbarosie, A.-M. Toader, Sensitivity of the homogenized coefficients with respect to variations of the microgeometry, ICCS16 - 16$^{\text{th}}$ International Conference on Composite Structures, Porto, 28-30 June 2011

[6] C. Barbarosie, A.-M. Toader, Optimization of the homogenized coefficients with respect to the microgeometry of holes, ICCE-21 The twentyfirst Annual International Conference on Composites and Nano Engineering, Tenerife, Spain, July 21-27, 2013

[7] C. Barbarosie, A.-M. Toader, Shape and Topology Optimization for periodic problems, Part I, The shape and the topological derivative, *Structural and Multidisciplinary Optimization*, 40, p. 381-391, 2009

[8] C. Barbarosie, A.-M. Toader, Shape and Topology Optimization for periodic problems, Part II, Optimization algorithm and numerical examples, *Structural and Multidisciplinary Optimization*, 40, p. 393-408, 2009

[9] O. Pantz, K. Trabelsi, A post-treatment of the homogenization method for shape optimization, *SIAM J. Control Optim.*, 47, p. 1380-1398, 2008

[10] C. Barbarosie, S. Lopes, A generalized notion of compliance, *Comptes Rendus Mécanique*, 339 (10), p. 641-648, 2011

[11] C. Barbarosie, Shape optimization of periodic structures, *Computational Mechanics*, 30, p. 235-246, 2003

[12] `http://cmaf.ptmat.fc.ul.pt/~barbaros/en/examples-2013.html` (web page)

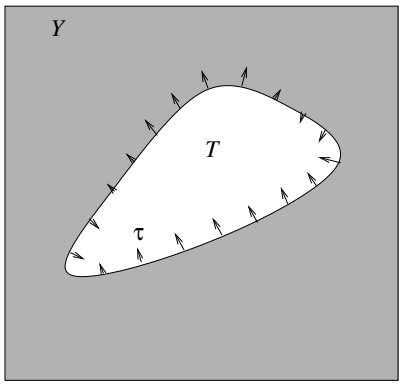

Figure 6: Infinitesimal deformation of the model hole T

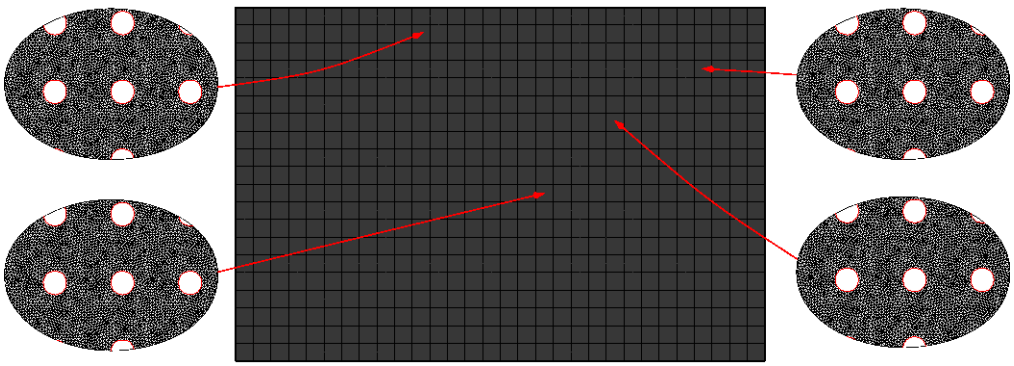

Figure 7: Initial guess

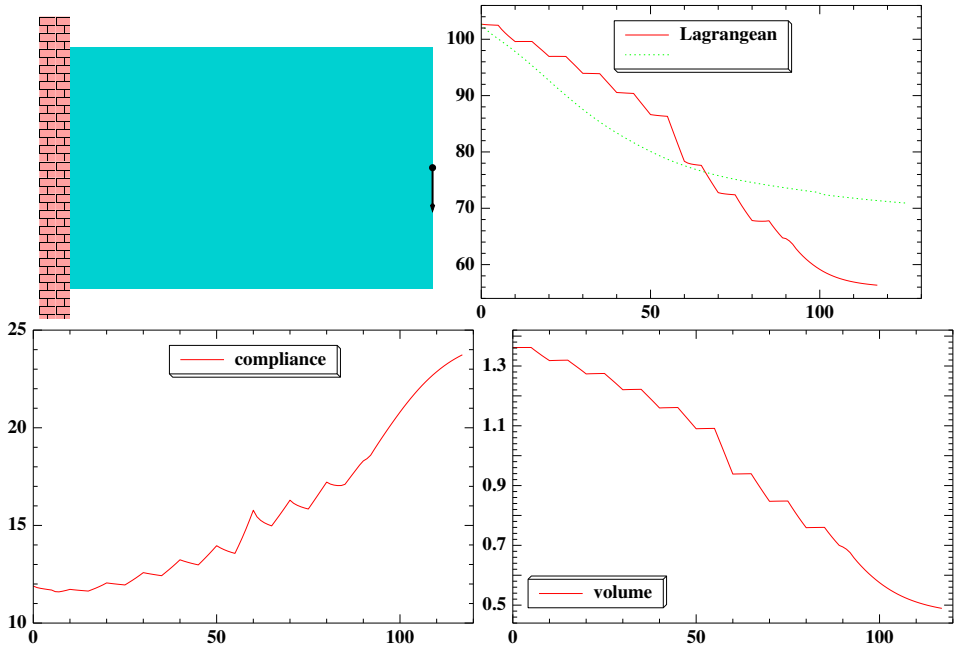

Figure 8: Cantilever with one load in the middle, problem setting and convergence history

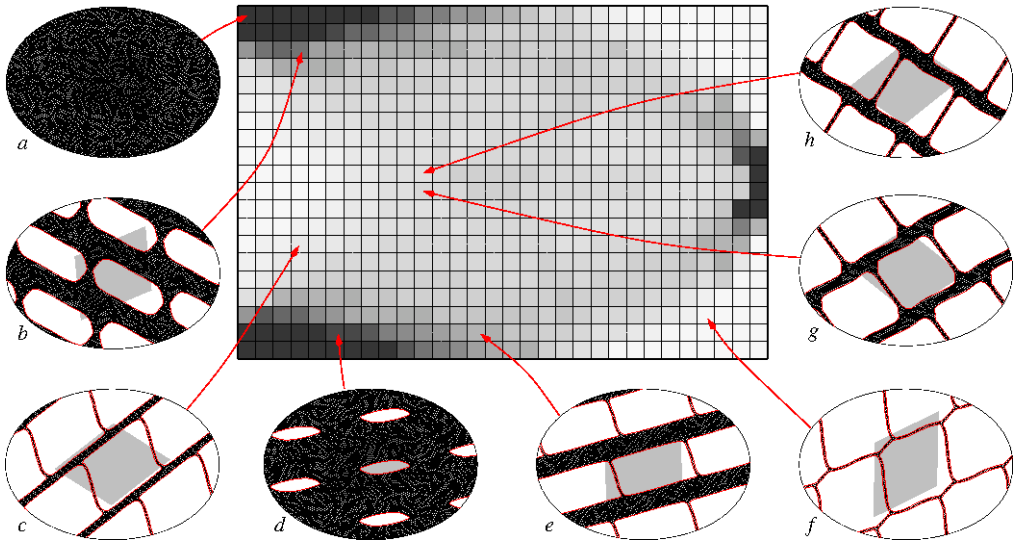

Figure 9: Cantilever with one load in the middle, optimized structure

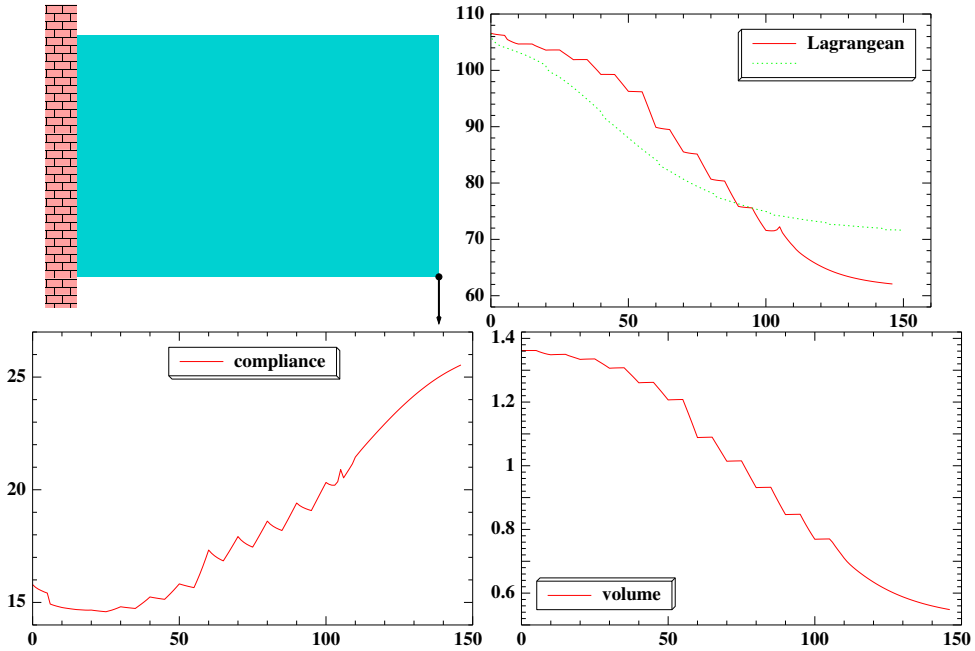

Figure 10: Cantilever with load in the lower corner, problem setting and convergence history

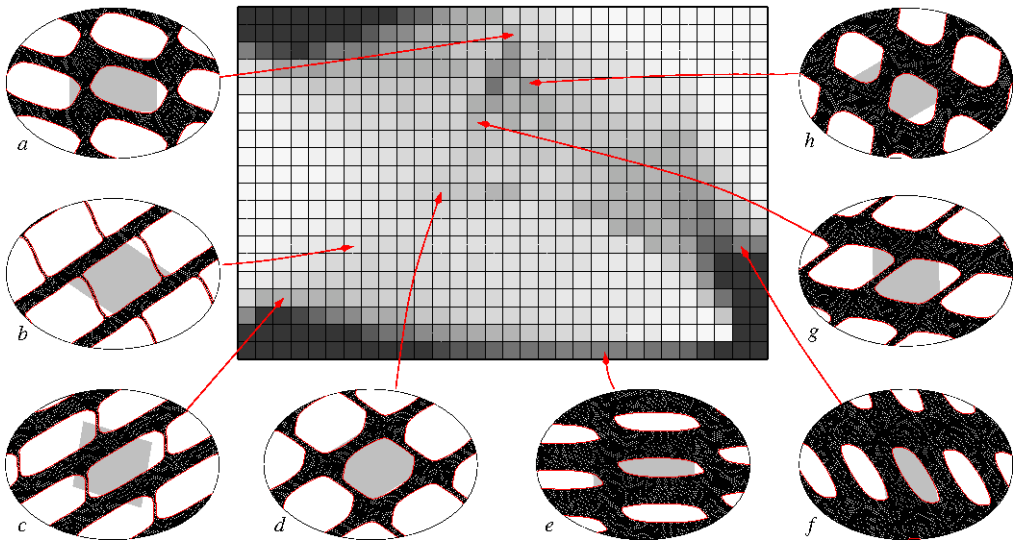

Figure 11: Cantilever with load in the lower corner, optimized structure

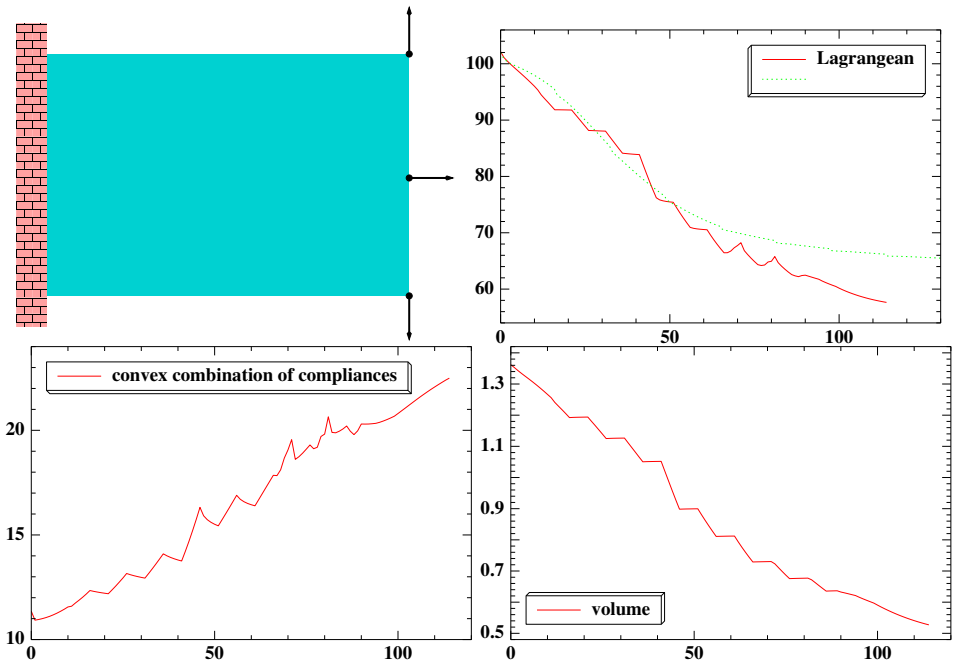

Figure 12: Cantilever with three independent loads, problem setting and convergence history

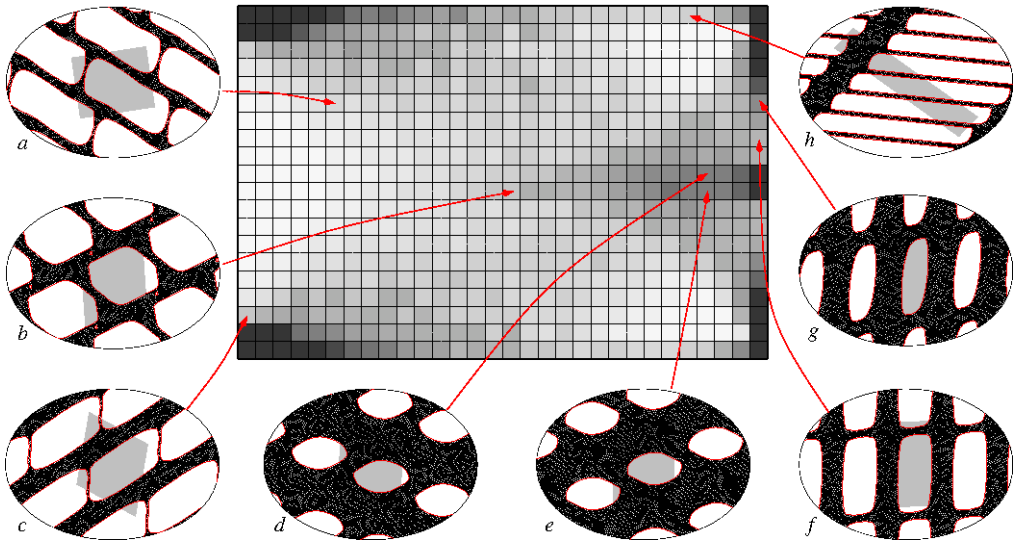

Figure 13: Cantilever with three independent loads, optimized structure